Journal of Molecular Structure 1074 (2014) 250–254

Contents lists available at ScienceDirect

Journal of Molecular Structure

journal homepage: www.elsevier.com/locate/molstruc

Growth and microstructural investigation of multiwall carbon nanotubes fabricated using electrodeposited nickel nanodeposits and chemical vapor deposition method

Navid Zanganeh [a], Armin Rajabi [b], Morteza Torabi [c], Masoud Allahkarami [d], Arshak Moghaddas [c], S.K. Sadrnezhaad [c,*]

[a] Mississippi State University, School of Chemical, Engineering, Mississippi State, MS 39762, USA
[b] Department of Materials Science and Engineering, Karaj Islamic Azad University (KIAU), Iran
[c] Department of Materials Science and Engineering, Sharif University, Tehran, Iran
[d] Mechanical and Aerospace Engineering, Oklahoma State University, Tulsa, OK, USA

HIGHLIGHTS

- Nickel nanodeposits were electrodeposited on n-Si(1 1 1):H substrate with a morphology of polygonal.
- The diffusion of carbon atoms in nano-particles Ni was acquired through decomposition of C_2H_2 at 700 °C.
- We were able to grow MWCNTs on nickel nanodeposits by CVD method.

ARTICLE INFO

Article history:
Received 7 March 2014
Received in revised form 4 June 2014
Accepted 4 June 2014
Available online 14 June 2014

Keywords:
Multiwall carbon nanotubes
Electrodeposition
Nickel nanodeposits
Chemical vapor deposition

ABSTRACT

This study proposes a common approach for growing multiwall carbon nanotubes (MWCNTs) on nickel nanodeposits. MWCNT growth was performed in two separate stages. In the first stage, nickel nanodeposits were electrodeposited on n-Si(1 1 1):H substrate in the presence of sulfuric acid. Based on atomic force microscopy (AFM) observations, the nickel deposits had a fairly polygonal morphology and were distributed on the prepared n-Si(1 1 1):H substrate. In the second stage, acetylene gas was decomposed on the surfaces of the nickel nanodeposits using chemical vapor deposition method at 700 °C. When carbon is saturated in a catalyst, it acts as a primary nucleating element for MWCNT growth. The structure of the MWCNTs was also investigated using scanning electron microscopy, high-resolution transmission electron microscopy, X-ray diffraction, and Raman spectroscopy. Results showed that the synthesized MWCNTs had a small wall thickness and were formed under the experimental conditions applied to the system.

Introduction

Although primary studies in the nanotechnology field have started since 1980, interest in nanoscience continues to grow because of various technological applications. These materials may bring significant innovation with their unique properties [1–4]. Carbon nanotubes (CNTs) are a group of relatively new nanomaterials made of carbon with a nanotubular structure and graphitic lattice [5]. CNTs possess attractive features, namely, electronic properties [6] and unique dimensions with a structural stability, because of efficient sp2 hybridization and p bonding [7]. These properties make them the best potential candidates in various fields of science and technology [8]. CNTs have potential applications in composite reinforcement [9], transistors [10], logic circuits [11], field emission sources [12], nano-biotechnology [13], and hydrogen storage nanodevices [14]. CNTs can be grown through different methods. The most common methods are direct current arc-discharge between electrodes [15], laser ablation of carbon rods [16], and chemical vapor deposition (CVD) [17]. CVD is preferred over the other techniques because of its high yield [18], high purity [19], low cost [20], and performance in irregular-shaped substrates and multiple-substrate coatings [21,22]. The main parameters for CNT growth via CVD are hydrocarbon sources, catalyst type, and growth temperature [22]. CNT growth mechanisms involve the dissociation of hydrocarbons catalyzed

* Corresponding author. Tel.: +98 21 66165215; fax: +98 21 66013126.
E-mail address: nanomaterialgroup@hotmail.com (S.K. Sadrnezhaad).

http://dx.doi.org/10.1016/j.molstruc.2014.06.012
0022-2860/

by transition metals and the saturation of carbon in a metal nanoparticle. Carbon precipitates from saturated metal nanoparticles and forms nano tubes [23]. The most effective catalysts for growing of CNTs known so far include iron, cobalt, and nickel [24]. The peculiar abilities of these metals are reportedly related to their catalytic activity for the carbon precursor decomposition, meta-stable carbide formation, carbon diffusion, and graphitic sheet formation [25,26]. Based on investigations on the average growth rate of CNTs in Fe, Co, and Ni catalysts through CVD, Ni catalysts have shown maximum growth rates [27]. The diffusion coefficients of carbon in bulk Fe, Co, and Ni metals are reported to be 1.1×10^{-7}, 8×10^{-8}, and 1.6×10^{-7} $cm^2\ s^{-1}$ at 950 °C, respectively. The diffusion rate of carbon follows the order of Ni > Fe > Co because it is usually proportional to the aforementioned metal diffusion coefficients [28]. Significant efforts have been devoted for growing CNTs on the Ni particles through chemical vapor deposition (CVD). It might be due to the fact that the survival of Ni nano particles associated with their size in the plasma method during CNT growth, i.e., small particles of Ni (<50 nm) were removed [29]. Generally, CNTs consist of two main groups': single-wall carbon nanotube (SWCNT) and multi-wall-carbon nanotube (MWCNT). In the present work, we highlight a common method (CVD) to grow MWCNTs on nickel nanodeposits that are electrochemically synthesized on well-defined n-Si(1 1 1):H electrode as catalyst through CVD.

Experimental details

The nickel nanodeposits used as catalyst for the growth of nano tubes were electrochemically prepared on an n-Si(1 1 1):H substrate. The n-Si(1 1 1):H substrate cleaned using the RCA procedure [30] before the electrodeposition process. During this process, degreasing in 2-propanol under reflux for 2 h was followed by alternate boiling in basic and acidic H_2O_2 solutions (NH_3:H_2O_2:H_2O = 1:1:5 and HCl:H_2O_2:H_2O = 1:1:5) for 15 min. The samples were etched for 1 min in 50% HF to remove the oxide layer and for 3 min in 40% NH4F. The last step led to the formation of well-defined monohydride-terminated Si(1 1 1) [Si(1 1 1):H] surfaces with large and atomically flat terraces [30]. The electrochemical measurements and deposition were performed in a typical three-electrode cell using a platinum plate as counter electrode [31]. Nickel was electrodeposited from 0.1 M H_2SO_4 + 10^{-4} M $NiSO_4$ (Merck, Germany). Electrochemical experiments were performed using an Autolab potentiostat/galvanostat model PGSTAT30. The potentiostatic transients were recorded at time intervals of 10 seconds. The morphology of the electrodeposited nickel nanodeposits was observed under a scanning electron microscope. The resultant catalyst was placed in a horizontal furnace and heated up to the growth temperature (700 °C) under nitrogen and hydrogen flow at 10:1 ratio. Then, acetylene was injected at a flow rate of 60 ml/min for 30 min. The MWCNTs growth on Ni-deposited n-Si(1 1 1):H substrate analyzed using scanning electron microscopy (SEM; Hitachi S-4800 with bruker EDX system), High-resolution transmission electron microscopy (HRTEM; JEOL JEM-2010) and X-ray diffraction (XRD; Philips X'Pert diffractometer Endhoven). Room-temperature Raman spectroscopy (Thermo Nicolet) was used to obtain the overall information on the synthesized carbon materials.

Results and discussions

A potentiostatic method was utilized to investigate the mechanism of the electrodeposition of nickel nanodeposits. Fig. 1 shows the potentiostatic current transient curves in a wide range of cathodic potentials from −0.7 V to −1.3 V for the electrodeposition

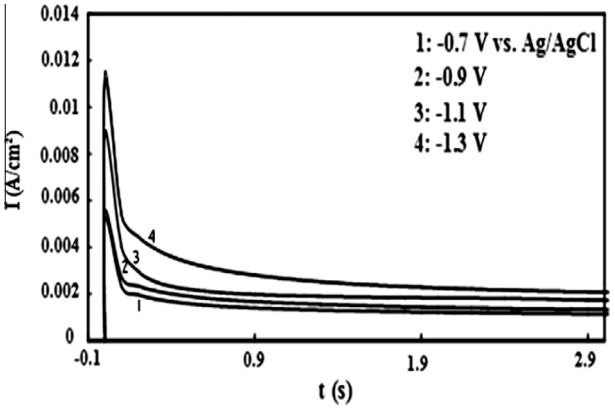

Fig. 1. Potentiostatic *I–t* transients for deposition of the nickel electrodeposition [31].

of nickel nanodeposits. The currents reached well-defined recognizable maxima observed as clear peaks because of the double layer capacitance. Then, a sharp fall and posterior growth occurred. The current densities of each transient increased with increasing overpotential.

According to the Pourbaix diagram of nickel [32], Ni is stable at this potential and pH range. The partial current related to Ni^{2+} reduction was lower than 1/1000 because of the low concentration of Ni^{2+} ions in the solution and the acidic pH. Moreover, the total current mainly increased from the proton reduction which simultaneously occurred. Therefore, inferring anything reliable on the nucleation and growth mechanism of the nickel electrodeposition from these transients is not possible. The surface morphology of the nickel deposits was observed under AFM. The AFM image of the nickel nanodeposits in Fig. 2 shows that the electrodeposition process is not preferential and the particles are distributed on n-Si(1 1 1). The morphology of the deposits was polygonal-like, and these deposits seemingly grew epitaxially.

Carbon nanotubes

Fig. 3 shows a typical SEM image of the MWCNTs grown on electrodeposited nickel nanodeposits using the CVD method

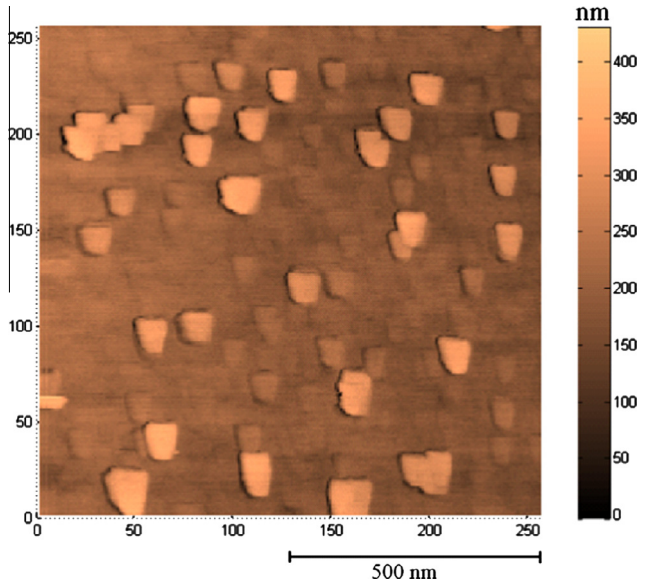

Fig. 2. AFM image of nickel nanodeposits electrodeposited on well-defined n-Si(1 1 1):H substrate.

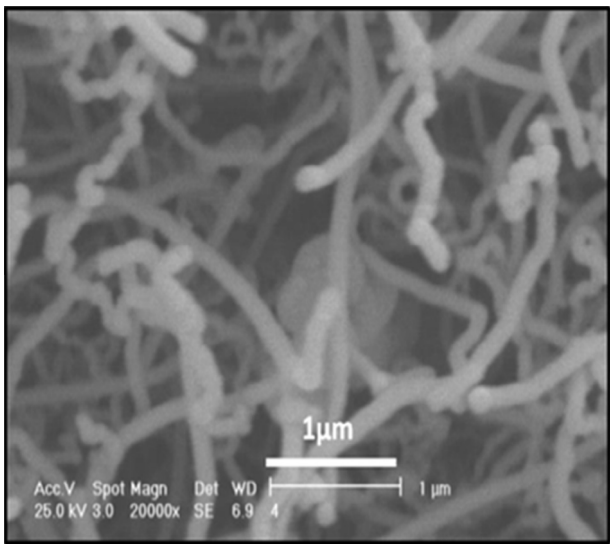

Fig. 3. SEM image of the MWCNTs grown on nickel nanodeposits electrodeposited on well-defined n-Si(1 1 1):H substrate.

(C_2H_2 gas, 30 min at 700 °C). The prepared MWCNTs are in various sizes of spaghetti-like shapes, long and curved. This model may be explained as follows. First, acetylene gas was decomposed on the surface of the nanometer-scale catalytic particles. Second, carbon

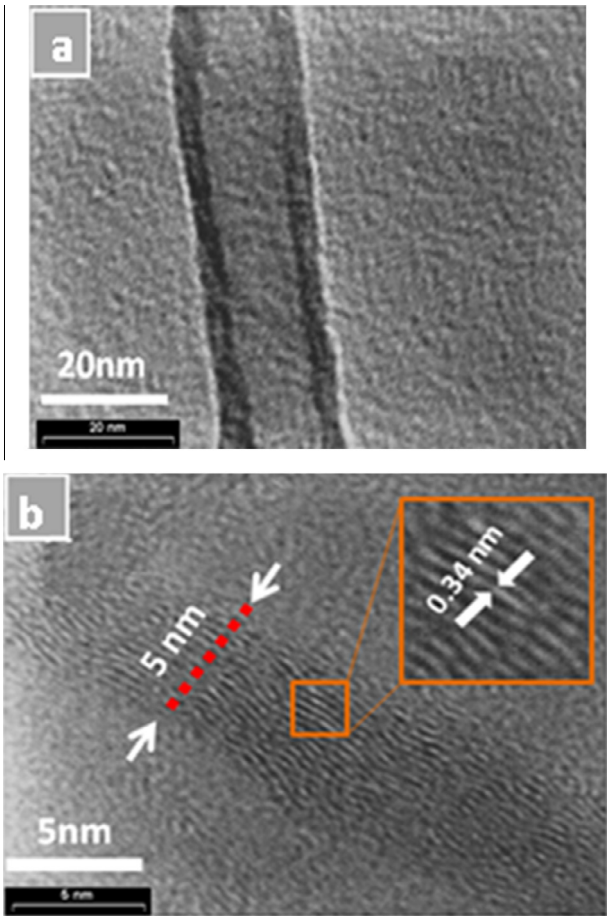

Fig. 4. HRTEM images of the MWCNTs grown on nickel nanodeposits electrodeposited on well-defined n-Si(1 1 1):H substrate. (a) Outside and (b) inside of MWCNTs.

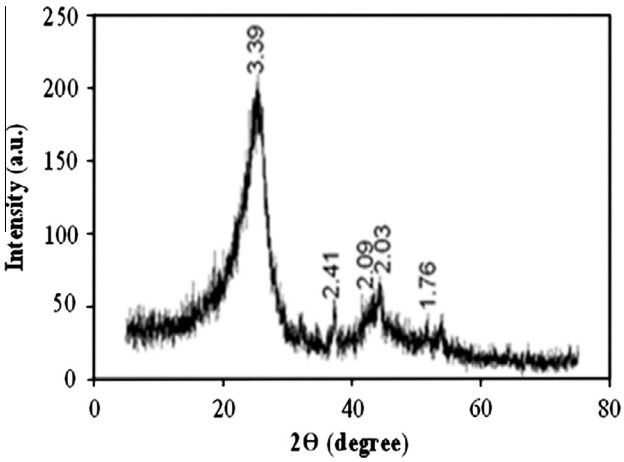

Fig. 5. XRD pattern of the MWCNTs grown on nickel nanodeposits electrodeposited on well-defined n-Si(1 1 1):H substrate.

was dissolved in the catalyst and diffused through it under an activity gradient. Finally, as the solubility of carbon was limited within the metal, carbon precipitated on the opposite side of the catalytic particle to form nano tubes with a graphitic structure [33]. Although the mechanism of CNT growth remains complicated, tip-growth mechanism is seemingly responsible for the

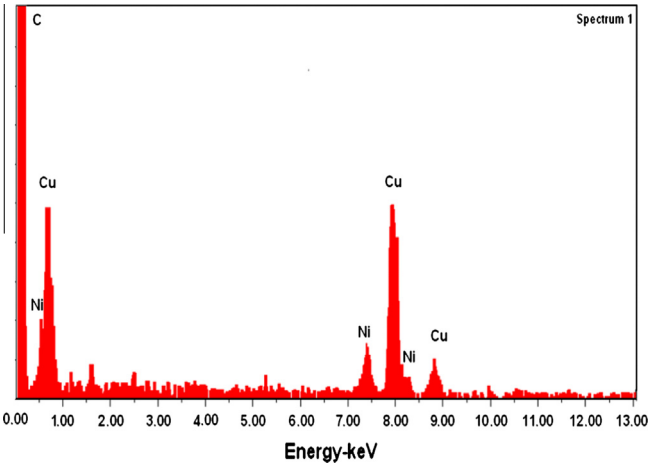

Fig. 6. EDX of the MWCNT grown on nickel nanodeposits electrodeposited on well-defined n-Si(1 1 1):H substrate.

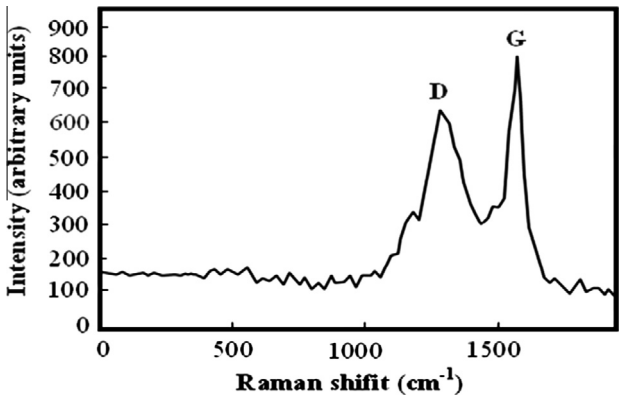

Fig. 7. Raman spectrum of the MWCNTs grown on nickel nanodeposits electrodeposited on well-defined n-Si(1 1 1):H substrate.

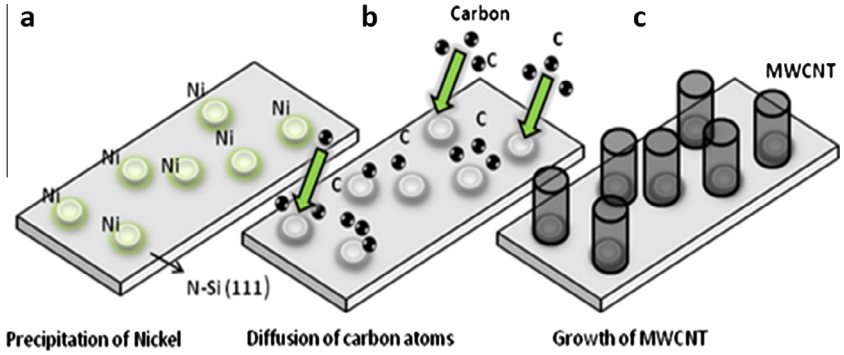

Fig. 8. Schematic progress of MWCNT manufactured through CVD method. (a) Precipitation of nano-nickel on n-Si(1 1 1):H substrate. (b) Diffusion of carbon atoms in nano-particles nickel. (c) Growth of MWCNT.

CNT synthesis [34,35]. Tube length increased when more carbons were deposited on the catalyst particles and diffused into or over the surface of the catalyst particles, incorporating into the graphitic lattice [36,37]. High-resolution transmission electron microscopy (HRTEM) was used to study the MWCNT in more details to support the SEM investigations. Fig. 4a and b shows a typical HRTEM image of outside-inside an MWCNT to be 20 nm and 5 nm respectively. Also, the interlayer spacing of the MWCNT is clearly illustrated in the inset of Fig. 4 (0.34 nm). Fig. 5 shows the XRD pattern of the multi-walled MWCNTs. The crystal structure and orientation of the nano tubes were investigated using Cu Kα radiation ($\lambda = 0.154178$ nm) as the main peak, and the (0 0 2) peak was observed at $2\theta = 25.43$. According to Bragg's equation [38], the space between (0 0 2) planes in crystals was calculated to be approximately 0.339 nm. In addition, the MWCNTs fabricated in this study have a structure similar to graphite [39].

Hitachi S-4800 SEM with bruker EDX system was used to characterize the purity of carbon nano tubes. In order to find the real amount of impurities, no additional washing, filtering and drying were perform before EDX analysis. Apart from Ni which was used as catalyst, the EDS results did not evidenced significant amount of impurities in the produced nanotube samples. It is practically impossible to completely eliminate the Ni from the samples with chemical treatment. The representative EDX presented in Fig. 6 shows that Nickel is the only impurities that can be found in the sample. Cu signals come from the copper grid. A trace amount of Silicon up to maximum 0.08%, S up to 0.02% and Na up to 0.05% were also detected.

Fig. 7 presents the Raman spectrum of the prepared MWCNTs. Raman spectra usually exhibit three characteristic bands, i.e., tangential stretching G mode, D mode and the radial breathing mode (RBM) [40]. Here, no (RBM) peaks were observed in frequency less than 500 cm^{-1}. Due to the RBM signal from large diameter tubes is usually too weak to be observable which revealed nanotubes obtained must be multiwall instead of single wall nanotube. The band at 1580 cm^{-1} is the G mode corresponding to the vibration of two sp2-bonded carbon atoms in a two dimensional (2D) hexagonal lattice, such as in a graphene sheet. This peak is related to a graphite E_{2g} mode. The 1320 cm^{-1} band is assigned to the D mode, which is not originally a Raman active mode of the graphene layer. This band is generally attributed to the defects in the curved graphene layers, tube ends, and staging disorder. The D-band is associated with vibrations of carbon atoms with dangling bonds in plane terminations of disordered graphite or glassy carbons. The intensity ratio of ID/IG that depends on the structural characteristics of MWCNTs is a usual measurement of graphitic ordering. The ID/IG value of the spectrum suggests a defective structure or a lower degree of graphitization in the MWCNT structure [41]. The (ID/IG) ratio for the as-grown MWCNTs, in this study, was ~0.80, which reveals the MWCNTs are not perfectly crystalline. This may be induced by low growth temperature of MWCNTs at 700 °C [42]. According to the analysis carried out by [43], the structure that corresponds to 1540 cm^{-1} to 1600 cm^{-1} can be explained by the z1-folding of the graphite phonon dispersion relation.

Fig. 8 schematically displays how MWCNTs were grown on polygonal nano nickel. The first schematic (Fig. 8a) shows nano nickel depositions on n-Si(1 1 1):H substrate, which were achieved through electroplating. The C_2H_2 decomposition at 700 °C resulted in the diffusion of carbon atoms in the nano nickel particles (Fig. 8b). Finally, carbon precipitation onto nickel grains favors nanostructure growth and results in the formation of MWCNTs (Fig. 8c). Based on literature, nano tubes carbon were grown along the vertical axis on the Ni particles, not at the interface between the nickel and silicon [44].

Conclusion

This study investigated the application of a special shape of nickel nanodeposits as catalysts for the high-yield preparation of high purity MWCNTs with desirable nanostructure. Using cyclic voltammetry to characterize the electrochemical behavior of the system, the nickel nanodeposits were electrodeposited on well-defined n-Si(1 1 1):H substrate in the presence of sulfuric acid. The spaghetti-like MWCNTs with small wall thickness were prepared using the CVD method.

References

[1] L. Zhang, T.J. Webster, Nano Today 4 (2009) 66–80.
[2] N. Zanganeh, S. Zanganeh, A. Rajabi, M. Allahkarami, R. Rahbari Ghahnavyeh, A. Moghaddas, M. Aieneravaie, S. Sadrnezhaad, J. Coord. Chem. (2014) 1–14.
[3] A. Rajabi, M. Aieneravaie, V. Dorosti, S. Sadrnezhaad, Materials Technology: Advanced Performance Materials (2014). doi/abs/10.1179/1753555714Y.0000000138.
[4] M. Razavi, M. Rahimipour, A. Rajabi, Mater. Sci. Technol. 28 (2013) 145–154.
[5] S. Iijima, Nature 354 (1991) 56–58.
[6] J. Yuan, Y. Huang, J. Mol. Struct. (Theochem) 942 (2010) 88–92.
[7] R. Zhang, S. Lee, C.K. Law, W.K. Li, B.K. Teo, Chem. Phys. Lett. 364 (2002) 251–258.
[8] M. Parthasarathy, J. Debgupta, B. Kakade, A.A. Ansary, M. Islam Khan, V.K. Pillai, Anal. Biochem. 409 (2011) 230–235.
[9] A. Fraczek-Szczypta, E. Dlugon, A. Weselucha-Birczynska, M. Nocun, M. Blazewicz, J. Mol. Struct. 1040 (2013) 238–245.
[10] A.D. Franklin, N.A. Bojarczuk, M. Copel, Appl. Phys. Lett. 102 (2013) 013104–013108.
[11] J. Zhang, N.P. Patil, A. Hazeghi, H.S.P. Wong, S. Mitra, IEEE Transactions on 30 (2011) 1103–1113.
[12] A.A. Kuznetzov, S.B. Lee, M. Zhang, R.H. Baughman, A.A. Zakhidov, Carbon 48 (2010) 41–46.
[13] X. Zhang, X. Wang, Q. Lu, C. Fu, Carbon 46 (2008) 453–460.
[14] Z. Zhang, T. Li, Appl. Phys. Lett. 97 (2010) 081903–081909.
[15] A. Thess, R. Lee, P. Nikolaev, H. Dai, P. Petit, J. Robert, C. Xu, Y.H. Lee, S.G. Kim, A.G. Rinzler, Science 273 (1996) 483.

[16] A. Dillon, K. Jones, T. Bekkedahl, C. Kiang, D. Bethune, M. Heben, Nature 386 (1997) 377–379.
[17] J. Safari, S. Gandomi-Ravandi, J. Mol. Struct. (2014).
[18] H. Kimura, J. Goto, S. Yasuda, S. Sakurai, M. Yumura, D.N. Futaba, K. Hata, ACS Nano 7 (2013) 3150–3157.
[19] Y.S. Kim, K. Kumar, F.T. Fisher, E.H. Yang, Nanotechnology 23 (2012) 015301.
[20] J. Huang, Q. Zhang, M. Zhao, F. Wei, Chin. Sci. Bull. 57 (2012) 157–166.
[21] K. Samant, S. Haram, S. Kapoor, Pramana 68 (2007) 51–60.
[22] T. Li, K. Kuwana, K. Saito, H. Zhang, Z. Chen, Proc. Combust. Inst. 32 (2009) 1855–1861.
[23] R. Brukh, S. Mitra, J. Mater. Chem. 17 (2006) 619–623.
[24] A. Mathur, S. Roy, C. Dickinson, J. McLaughlin, Curr. Appl. Phys. 10 (2010) 407–410.
[25] A.N. Andriotis, M. Menon, G. Froudakis, Phys. Rev. Lett. 85 (2000) 3193–3196.
[26] C.H. Kiang, J. Phys. Chem. A 104 (2000) 2454–2456.
[27] C.J. Lee, J. Park, J.A. Yu, Chem. Phys. Lett. 360 (2002) 250–255.
[28] R. Baker, M. Barber, P. Harris, F. Feates, R. Waite, J. Catal. 26 (1972) 51–62.
[29] Y. Tu, Z. Huang, D. Wang, J. Wen, Z. Ren, Appl. Phys. Lett. 80 (2002) 4018–4020.
[30] W. Kern, RCA Review 31 (1970) 187–206.
[31] M. Torabi, R. Khalifehzadeh, H. Arami, S. Sadrnezhaad, IJE. B 21 (2008) 177.
[32] B. Beverskog, I. Puigdomenech, Corros. Sci. 39 (1997) 969–980.
[33] C.P. Deck, K. Vecchio, Carbon 43 (2005) 2608–2617.
[34] K. Teo, S. Lee, M. Chhowalla, V. Semet, V.T. Binh, O. Groening, M. Castignolles, A. Loiseau, G. Pirio, P. Legagneux, Nanotechnology 14 (2003) 204.
[35] M. Kumar, Y. Ando, J. Nanosci. Nanotechnol. 10 (2010) 3739–3758.
[36] R. Brukh, S. Mitra, J. Mater. Chem. 17 (2007) 619–623.
[37] T. Chieu, M. Dresselhaus, M. Endo, Phys. Rev. B 26 (1982) 5867.
[38] X. Wang, D. Zhang, H. Zhang, Y. Ma, J.Z. Jiang, Nanotechnology 22 (2011) 305306.
[39] Z. Huang, A. Calka, H. Liu, J. Mater. Sci. 42 (2007) 5437–5441.
[40] S. Osswald, M. Havel, Y. Gogotsi, J. Raman Spectrosc. 38 (2007) 728–736.
[41] Y. Homma, Y. Kobayashi, T. Ogino, D. Takagi, R. Ito, Y.J. Jung, P.M. Ajayan, J. Phys. Chem. B 107 (2003) 12161–12164.
[42] Z. Liu, G. Yang, Y.Z. Lee, D. Bordelon, J. Lu, O. Zhou, Appl. Phys. Lett. 89 (2006) 103111–103113.
[43] A. Kasuya, Y. Sasaki, Y. Saito, K. Tohji, Y. Nishina, Phys. Rev. Lett. 78 (1997) 4434.
[44] Z. Ren, Z. Huang, D. Wang, J. Wen, J. Xu, J. Wang, L. Calvet, J. Chen, J. Klemic, M. Reed, Appl. Phys. Lett. 75 (1999) 1086–1088.